Air Force Institute of Technology

AFIT Scholar

12-2-2019

Effect of Surface Roughness on Ultrasonic Inspection of Electron Beam Melting Ti-6AL-4V

Evan T. Hanks

Anthony N. Palazotto
Air Force Institute of Technology

David Liu

Follow this and additional works at: https://scholar.afit.edu/facpub

Part of the Materials Science and Engineering Commons

Recommended Citation

Hanks, E., Palazotto, A., & Liu, D. (2019). Effect of surface roughness on ultrasonic inspection of electron beam melting ti-6AL-4V. Journal of Defense Analytics and Logistics, 3(2), 131–141. https://doi.org/10.1108/JDAL-12-2018-0019

Effect of surface roughness on ultrasonic inspection of electron beam melting ti-6AL-4V

Evan Hanks, Anthony Palazotto and David Liu

Department of Aeronautics and Astronautics, Air Force Institute of Technology, Wright Patterson AFB, Ohio, USA

Abstract

Purpose – Experimental research was conducted on the effects of surface roughness on ultrasonic non-destructive testing of electron beam melted (EBM) additively manufactured Ti-6Al-4V. Additive manufacturing (AM) is a developing technology with many potential benefits, but certain challenges posed by its use require further research before AM parts are viable for widespread use in the aviation industry. Possible applications of this new technology include aircraft battle damage repair (ABDR), small batch manufacturing to fill supply gaps and replacement for obsolete parts. This paper aims to assess the effectiveness of ultrasonic inspection in detecting manufactured flaws in EBM-manufactured Ti-6Al-4V. Additively manufactured EBM products have a high surface roughness in "as-manufactured" condition which is an artifact of the manufacturing process. The surface roughness is known to affect the results of ultrasonic inspections. Experimental data from this research demonstrate the ability of ultrasonic inspections to identify imbedded flaws as small as 0.51 mm at frequencies of 2.25, 5 and 10 MHz through a machined surface. Detection of flaws in higher surface roughness samples was increased at a frequency of 10 MHz opposed to both lower frequencies tested.

Design/methodology/approach – The approach is to incorporate ultrasonic waves to identify flaws in an additive manufactured specimen

Findings – A wave frequency of 10 MHz gave good results in finding flaws even with surface roughness present.

Originality/value – To the best of the authors' knowledge, this was the first attempt that was able to identify small flaws using ultrasonic sound waves in which surface roughness was present.

Keywords Nondestructive inspection (NDI), Nondestructive testing (NDT), Nondestructive evaluation (NDE), Electron beam melting (EBM), Ti-6Al-4V, Additive manufacturing (AM)

Paper type Research paper

1. Introduction

Electron beam melting (EBM) is a direct digital manufacturing (DDM) technique, capable of producing near-net-shape parts from powdered metal. The EBM technology has the ability to build dense parts using a fully automated computer-controlled system with minimal

interaction during the build process (Safdar, 2012). As with most additive manufacturing (AM), the buildup process starts with a computer aided design (CAD) model (Energetics Incorporated, 2013). The model is then digitally sliced into layers and physically reproduced layer by layer through the melting of powdered metal, which produces the desired shape (Safdar, 2012). AM is a rapidly growing industry because of an expanding material selection; these materials include various steel, aluminum and titanium alloys (Ruan, 2006; Ford, 2014; Shipp, 2012). The growth of available materials from simple low-strength plastics to high-strength alloys has opened the door to custom, as needed, manufacturing of components.

Certain roadblocks stand in the way of on-demand AM parts. The first of these barriers is the need for a process to qualify parts for use in an assembly. Traditional production run sampling and first article testing can add significant time and money to the cost of spares. For low number productions, where AM has the most benefit, this qualification process could negate any potential cost or time savings (Shipp, 2012). Among the challenges to qualify AM components for use is the need for nondestructive inspection of finished products. Inspection is needed both prior to use and throughout the life cycle of the system in which they are used. The avenue to validate, verify and qualify AM parts is of universal concern throughout the industry, as well as throughout the government. Adoption of parts made by AM is hampered by doubt in the current nondestructive inspection (NDI)-based validation approaches. Current NDI methods are not optimized for AM materials or processes. The use of traditional NDI techniques for completed AM components are either untested or still emerging (Waller, 2014). In 2013, the National Institute of Standards and Technology (NIST) laid out a roadmap for metal-based AM. Included in this document was a five-year action plan to explore and develop NDI techniques and protocols. One of the first steps outlined by the NIST is to benchmark AM measurements, accuracies and NDI techniques to enable process performance validation (Energetics Incorporated, 2013). Current industry and government research is split into two distinct categories, *in situ* process NDI and post process NDI. The focus of *in situ* NDI is to provide real-time effective feedback to the AM equipment, allowing for the detection or mitigation of anomalies (Energetics Incorporated, 2013). Post-process NDI is also a concern and is laid out in the five-year plan of evaluation and development by the NIST. This plan calls for proven techniques, based on adapting existing NDI practices, to meet the needs of AM (Energetics Incorporated, 2013).

Other works recently published focus on the inspection of samples manufactured using laser-melted powder or election beam-melted wire. These previous works used laser ultrasonic with synthetic aperture focusing to detect lack of bonding and lack of fusion. As with the work presented in this paper, other research has used CT inspections to confirm UT results (Levesque, 2016). Previous works focus on the feasibility of ultrasonic inspection on AM materials; this research will begin to investigate the factors which affect the ability to detect internal flaws in EBM materials.

The purpose of this research is to investigate the effect of surface roughness on ultrasonic nondestructive testing (UT) of EBM Ti-6Al-4V. Owing to the variability in manufacturing using EBM, surface finish is often less than desirable for traditional forms of NDI (Hanks, 2016). Additional data will help develop a greater understanding of inspection technique and surface finish requirements. Surface conditions tested in this paper are representative of parts in an as-manufactured condition, as well as those which have received post-process machining. Given the lack of reliable analytical data to correlate surface roughness to flaw detection using NDI, this research will attempt to determine the

extent to which surface finish causes a measurable difference in flaw detection of EBM titanium alloy samples at frequencies of 2.25, 5 and 10 MHz.

2. Material and methods

The specimens used in this testing were designed by the structural materials division of the air force research laboratory (AFRL) for the purpose of nondestructive testing, as well as destructive inspection techniques. The samples were designed as rectangular blocks 25.4-mm wide (Y), 25.4-mm tall (Z) and 114.3-mm long (X) represented in Figure 1. Specimens were designed and built as sets of two exactly similar samples in each production run. Each block was designed with five embedded spherical flaws, ranging in size from 0.51 to 2.54 mm in diameter as listed in Table I. These flaws were designed on the center line of the sample, with the center of the spheres evenly spaced in ascending diameter as shown in Figure 2.

Samples used for this testing were made using one of two powder lots, both meeting the same specification and assumed to be constant for the research performed.

The six sets of samples used in this study were produced as six sets of two builds. Each production run, containing two samples, were given an alphabetic designation. Production runs A, B, D, E, L and M were used to collect UT data. Samples A to E were manufactured using Arcam's A2 system, with software version 3.2, while samples L and M were manufactured on Arcam's newer Q10 system. Samples were designated as −41 and −42 within each production run. All samples were manufactured with the X-axis of the sample parallel to the X-axis of the AM machine's powder bed. Data were collected from these 12 samples in four configurations: as manufactured top surface, as manufactured side surface, milled top surface and milled side

Figure 1.
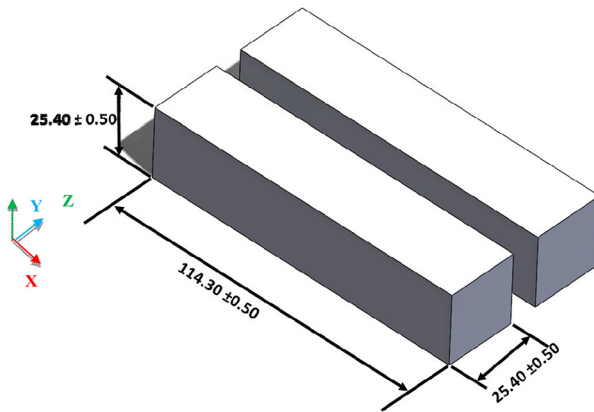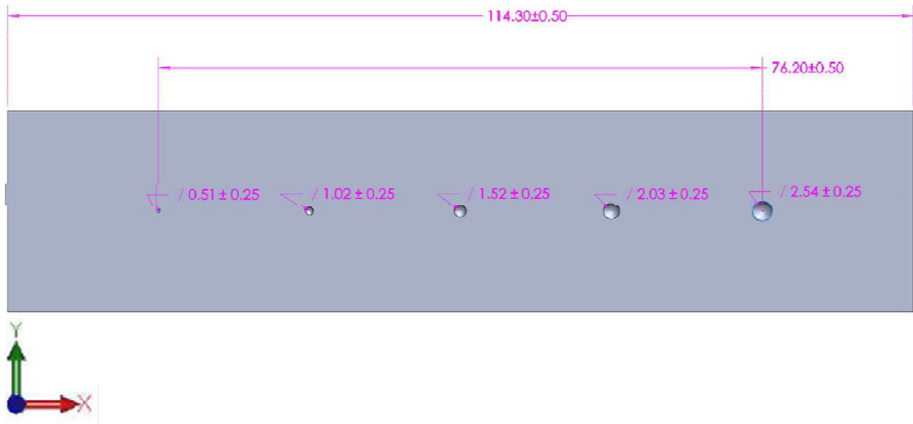Design of samples

Flaw	Diameter (mm)	Diameter (in)
1	0.51	0.020
2	1.02	0.040
3	1.52	0.060
4	2.03	0.080
5	2.54	0.100

Table I.
Sample designed
flaw dimensions

Figure 2.
CAD design of
samples to include
defects, plain view
and dimensions in
mm

surface. This provided a minimum of four surface finishes from which to collect data on each of
the 12 samples, as well as two potentially different powder lot configurations.

The build process resulted in relatively smooth bottom and top surfaces and much
rougher surfaces normal to the X-Z and Y-Z planes. Measurements were performed using a
Taylor–Hobson Form Talysurf model 120 surface profilometer. The measurement area was
10-mm long and 10-mm wide of the 114.3-mm-long and 25.4-mm-wide surface, respectively.
Each surface roughness scan collected 1,000 points in which to calculate surface roughness.
These data points were used by the built-in software of the profilometer to calculate the root
mean square (RMS) of the surface roughness. A linear profile of the top surface is seen in
Figure 3.

The Taylor–Hobson Form Talysurf 120 has a maximum range of 120 μm. Following
multiple attempts to measure the side surface, X-Z plane, with this particular profilometer,
the surface was determined to be above the range of measurement. Alternate methods of
measurement were explored; the method ultimately chosen was a 3D measuring
macroscope. The 3D measuring macroscope provided similar results to the profilometer.
Two top surfaces were measured with both the profilometer and the measuring macroscope.
A difference of approximately 4 per cent and 0.2 per cent in surface roughness was found
between the two measurement methods on these samples. It was assumed that samples
from the same production run, both sample - 41 and -42, have the same side surface
roughness. Table II provides surface roughness measurements for the as-manufactured
surfaces of each sample.

Figure 3.
Linear profile of
sample A-41, top
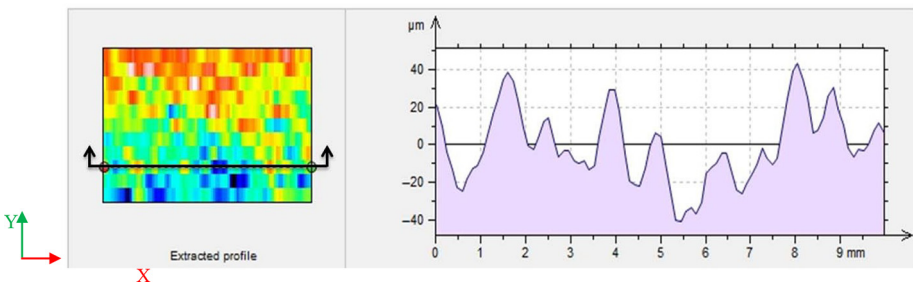surface in X-Z plane
with roughness of
16.8 μm RMS

Sample	Top surface (μm) rq	Top max peak to valley (μm)	Side surface (μm) rq	Side max peak to valley (μm)
A-41	16.8	115.3		
A-42	16.1	102.6	45.1	307
B-41	22	103.8		
B-42	21.2	127	40.9	268.5
D-41	19.6	118.5		
D-42	18.8	118.7	58.7	439.1
E-41	16.2	83.6		
E-42	15.5	93.7	43.78	320.1
L-41	11.1	71.3		
L-42	16.5	101.7	25.46	202.8
M-41	18.3	88		
M-42	15.8	99.8	27.03	208.9

Table II.
Sample surface
roughness
measurements prior
to machining

Ultrasonic inspections were completed on all 12 samples at 2.25, 5 and 10 MHz, both through the top and side surfaces. Focused beam transducers were selected for each of these frequencies. A focal length of 7.62 cm was available in each frequency. Focal length is the distance from the point in which the beam is concentrated to the face of the transducer, through a specific medium. The velocity of the longitudinal wave in water is 149,860 cm/sec, and 609,600 cm/sec in titanium, which causes the beam to focus or converge on a point faster in titanium resulting in a shorter focal length (Department of Defense, 2014). The samples under inspection are 2.54 cm in thickness with the flaws located on the centerline as described previously. Given the velocity of the wave in titanium is four times that of water, the equivalent focal length from the surface to the centerline of the sample is 5.08 cm. With a 7.62 cm focal length transducer placed 2.54 cm above a sample submerged in distilled water the focal point is in the optimal position for the designed flaws.

The transducer was mounted to a three-axis translational stage allowing full computer control of the transducer. The traverse is mounted over an immersion tank where distilled water was used as a couplant for the inspection. A leveling plate was then used to ensure the surface under inspection was in a horizontal orientation during scanning. The Z-axis was set to focus the beam on the centerline of each sample and held constant throughout each scan. The primary scan axis was designated as the X-axis with a collection interval of 0.06 mm, providing a minimum of 8 points across the smallest known flaw. The secondary scan axis was the Y-axis, also with a 0.06 mm step size. Each set of scans resulted in 857,286 A-scans per sample. The raw output A-scans were gated to produce C-scans of each sample. The C-scan is 256 grayscale image intensities of peak return amplitudes at the gated time window. The middle 0.635 cm of each sample was isolated to provide a C-scan of the center region, as shown in Figure 4.

Upon completion of UT on all as-manufactured specimens, post process machining was accomplished. One sample of each set of specimens, −41, was selected to have the upper and side surfaces milled smooth. Sample −42 of each set was not machined and held as a control, also allowing for future testing of as-manufactured specimens. A shell cutter was used on a three-axis mill to remove surface roughness. Post-machining surface roughness was measured and is shown in Table III for the top surface and Table IV for the side surface.

To evaluate the effects of surface roughness on the ability to detect flaws, a second set of ultrasonic tests were conducted. Samples were again inspected in sets of two, allowing for comparison with the original set of scans. UT was accomplished through both the top and

side surfaces. The same three transducers were used as in previous testing, producing frequencies of 2.25, 5 and 10 MHz grayscale images of the C-scans were processed through a series of image processing techniques to include "image erosion" using MATLAB's built-in image processing tools. Image erosion reduces the number of unusable high gradient pixels in regions smaller than the detectable area of the transducer (Hanks *et al.*, 2016). A circular Hough transform was then performed, again using MATLAB's built-in function, on the eroded image to identify the presence of the designed flaws. The Hough transform function in MATLAB outputs a red circle on the image identifying a circular area of maximum gradient (MathWorks, 2015). The use of the circular Hough transform is intended to produce a repeatable identification process while removing the human interpretation of the C-scan.

3. Results and discussion

Figure 5 provides a representative graph of the ability of the UT and data processing technique to detect the known defects in the Ti-6Al-4V EBM samples. In this graph, the ordinate provides the ratio of detected flaws (N) to the number of known flaws present (N). The abscissa gives the diameter of the designed flaws in the samples. Each designed flaw size has 36 inspections per frequency, comprising a variety of surface roughnesses, as well as inspection through perpendicular sample faces. From this graph, it is seen that a 10 MHz transducer provides a higher detectability throughout the range of flaw sizes. Lower frequencies, such as 2.25 and 5 MHz, provide lower detectability starting at a 0.51 mm flaw with a slight increase in detection as flaw size increases. Both 2.25 and 5 MHz reach a detectability near 0.75 despite the flaw size, with no regard to surface roughness. The

Figure 4.
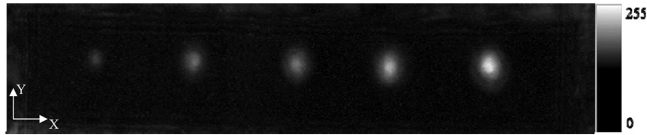Example of C-scan, center 0.635 cm of sample through top surface

Sample	RMS	Max valley	Max peak	Max peak to valley	RMS decrease (%)
A-41	3.2	8.3	9.1	17.4	80.8
B-41	5.0	12.6	8.2	20.8	77.2
D-41	3.2	8.5	7.7	16.3	82.8
E-41	3.9	15.1	9.7	24.7	76.2
L-41	1.9	4.3	5.1	9.4	83.2
M-41	3.7	6.0	7.7	13.7	79.7

Table III.
Surface roughness post machining, top surface (μm)

Sample	RMS	Max valley	Max peak	Max peak to valley	RMS decrease (%)
A-41	7.1	17.6	10.5	28.1	84.3
B-41	7.9	11.7	16.1	27.8	80.7
D-41	5.5	14.2	16.5	30.7	90.6
E-41	5.7	9.7	15.5	25.2	87.0
L-41	2.3	4.9	5.72	10.6	90.9
M-41	2.9	8.3	5.29	13.6	89.4

Table IV.
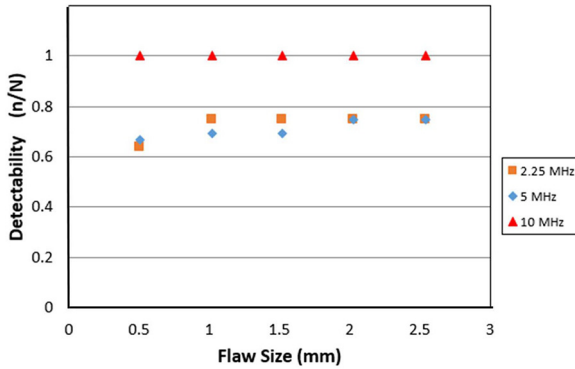Surface roughness post machining, side surface (μm)

Figure 5.
Detectability of flaws
by size and frequency
using UT

disparity between frequencies, as well as surface roughness factors, limiting detectability are explored in greater depth in Figures 6 and 7.

Figures 6 and 7 clearly show that for 2.25 and 5 MHz a higher percentage of the designed defects are detected at lower surface roughness. Analyzing these diagrams, several patterns are observed. For UT performed at 2.25 and 5 MHz, no defects were detected on a surface with a roughness greater than 40.9 μm. Using a 2.25 MHz transducer, 24 scans were conducted on surfaces with a roughness of less than 22 μm. These 24 scans inspected 120 instances of flaws and only failed to detect one designed defect. At a frequency of 5 MHz, all designed defects were detected through surface roughness of less than 22 μm. In the range of 22-27 μm, four scans were performed inspecting 20 defects, identifying 8 of the 20. This range appears as a transition zone. Above this range no defects were found and below this range all defects were identified at 5 MHz. An equivalent chart was not prepared for 10 MHz because all designed defects were identified in the samples tested regardless of surface roughness.

Figure 8(a-c) shows detected flaws through as manufactured surfaces of sample A-41, and Figure 8(d-f) denotes the flaws found in sample A-41 after machining. Comparing Figure 8(a-c) with Figure 8(d-f), machining appears to diminish the large areas of returns not associated with known flaws. This reduction is seen more at 2.25 MHz but exists at all
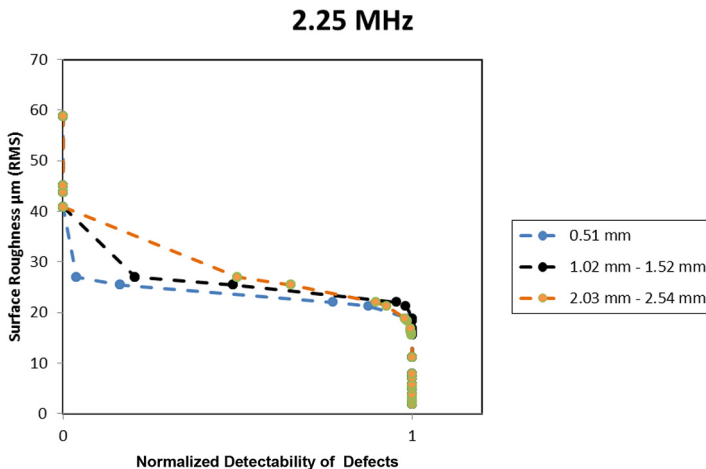

Figure 6.
Defects detected at
measured surface
roughness at
2.25 MHz

5 MHz

(a)   (b)   (c)   (d)   (e)   (f)
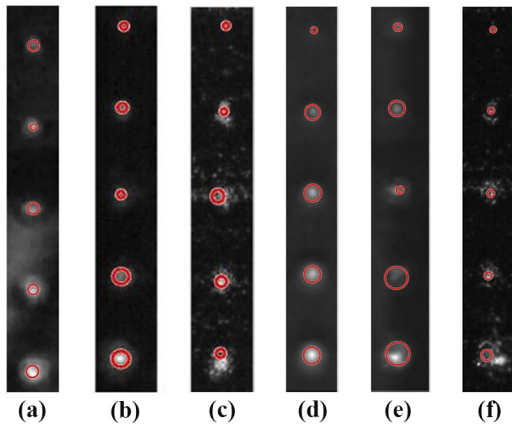
Notes: (a) 2.25 MHz as-manufactured; (b) 5 MHz
as-manufactured; (c) 10 MHz as-manufactured;
(d) 2.25 MHz milled; (e) 5 MHz milled; (f) 10 MHz
milled

frequencies. The decrease allows better distinction between designed defects and noise. The results seen in sample A-41 was typical of all samples manufactured on the Arcam A2 system. At this roughness , all flaws could be detected. The machining of these samples to a roughness of 3.22 μm RMS did not improve or degrade the identification of the flaws, as all were identified at the as-manufactured surface roughness.

Figure 9(a) and (b) shows results of the as-manufactured side surfaces at frequencies of 2.25 MHz and 5 MHz. As seen in Figure 9(a) and (b) no defects were detected through this side surface in as-manufactured condition, this result was observed on all side surfaces manufactured with the Arcam A2 system. Sample A-41 shown in Figure 8 had an as-
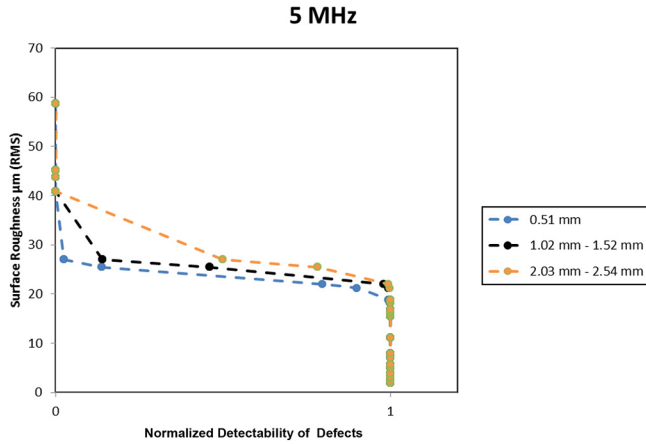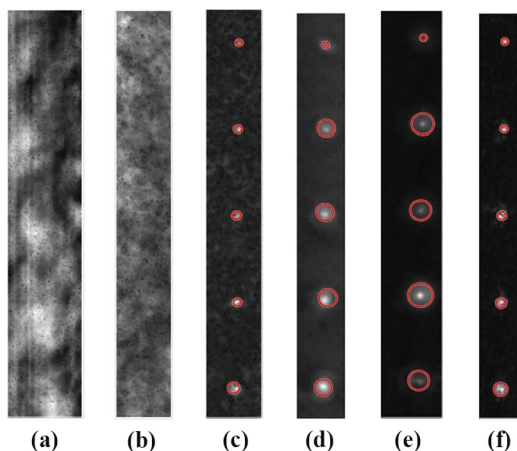
Notes: (a) 2.25 MHz as-manufactured; (b) 5 MHz
as-manufactured; (c) 10MHz as-manufactured;
(d) 2.25 MHz milled; (e) 5 MHz milled; (f) 10 MHz
milled

Figure 9.
Sample A-41 side
surface

manufactured surface roughness of 45.14 μm RMS once machining was accomplished on this surface of sample A-41 a roughness of 7.1 μm RMS was achieved. The side surfaces did provide usable returns at 2.25 and 5 MHz once the surfaces were machined. As shown in Figure 9(d) and (e) all designed defects are now visible and detectable using the circular Hough Transform. With the as-manufactured side surface's roughness of 45.14 μm and a peak to peak distance of 307 μm, no flaws were visible. However, with a reduction in roughness of 38 μm RMS, all designed spherical defects are identifiable via ultrasonic testing. This outcome was common across all samples from the Arcam A2 machine. Figures 9(c) and (f), collected using a 10 MHz transducer show much less influence in detection based on the change in roughness between surface condition.

Figure 10 provides a representative image of C-scans performed on samples manufactured on the Arcam Q10 system. Unlike samples manufactured on the A2, flaws could be detected through the as-manufactured side surface with a roughness of 25.46 μm RMS. At 2.25 MHz four of the five flaws were detected, while at 5 MHz two of the five designed flaws were detected through the as-manufactured surface. As noted on all sample side surfaces, more designed flaws and smaller designed flaws could be detected post-machining than in the as-manufactured condition. Machining of this sample reduced the side surface roughness from 25.46 to 2.32 μm RMS, once the machining was accomplished all flaws were detectable in this sample using ultrasonic testing. Table V provides an overview of the number of flaws detected in each configuration by designed flaw diameter. As shown in Table V only once did the ultrasonic test method used fail to identify a flaw in a post-manufacturing machined surface. This inability to identify only occurred once and was of the smallest flaw in the test. The results in this table also demonstrate the consistent ability of ultrasonic testing to identify flaws through an as manufactured top face (X-Y plane) of a sample. This table also illustrates the ability of higher frequency transducers to detect more flaws through a rougher as-manufactured side surface than lower frequency transducers.
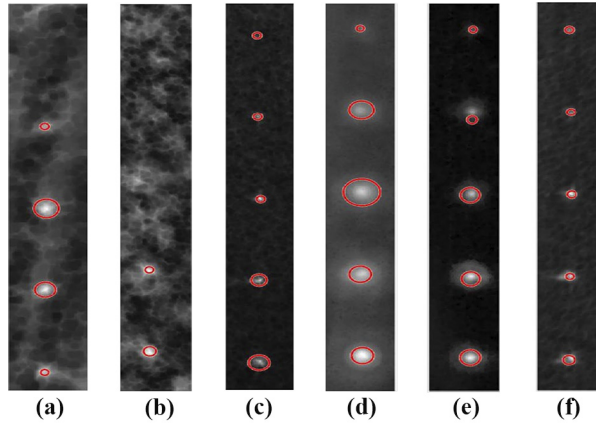
Figure 10.
Sample L-41 side
surface

Notes: (a) 2.25 MHz as-manufactured; (b) 5 MHz
as-manufactured; (c) 10MHz as-manufactured; (d) 2.25 MHz
milled; (e) 5 MHz milled; (f) 10 MHz milled

Frequency	Condition		Flaw design diameter (mm) 0.51	1.02	1.52	2.03	2.54
2.25 MHz	As-manufactured	Top face	12/12	12/12	12/12	12/12	12/12
		Side face	0/12	4/12	4/12	4/12	4/12
	Milled	Top face	6/6	6/6	6/6	6/6	6/6
		Side face	5/6	6/6	6/6	6/6	6/6
5 MHz	As-manufactured	Top face	12/12	12/12	12/12	12/12	12/12
		Side face	0/12	1/12	1/12	3/12	3/12
	Milled	Top face	6/6	6/6	6/6	6/6	6/6
		Side face	6/6	6/6	6/6	6/6	6/6
10 MHz	As-manufactured	Top face	12/12	12/12	12/12	12/12	12/12
		Side face	12/12	12/12	12/12	12/12	12/12
	Milled	Top face	6/6	6/6	6/6	6/6	6/6
		Side face	6/6	6/6	6/6	6/6	6/6

Table V.
Number of designed
defects detected

Through the process of an ultrasonic inspection the sound wave emitted by the transducer
passes through the couplant as described in earlier sections. Once the wave passes through the
couplant it contacts the surface of the sample under inspection. The roughness of the surface
causes a dispersion of the sound wave's pressure. A portion is reflected in varying directions
while another portion is scattered within the sample. As discussed by İŞLEYİCİ the amplitude
of the returned signal does not decrease proportionally to surface roughness but must be
considered (İŞLEYİCİ, UMUT, 2005). İŞLEYİCİ also found lower frequencies produced more
favorable results on rougher surfaces up to a roughness of 26 μm (İŞLEYİCİ, UMUT, 2005).

4. Conclusions
Experimental data from this investigation indicate an overall improvement in detectability
of flaws using UT on EBM Ti-6Al-4V with reduction in surface roughness. At frequencies
of 2.25 and 5 MHz, the orientation of inspection surfaces, side vs top, appears to have no

impact on the ability to detect internal defects. However, surface roughness has a direct impact on the ability to identify defects at these low frequencies. As discussed in the previous section, an as-manufactured side surface with a roughness greater than 40.9 μm RMS provides no detection of defects. When the same surface is inspected after machining, through a surface roughness of less than 7.9 μm RMS, all designed defects were identified.

Inspections performed at 10 MHz produced high-intensity returns through side surfaces of samples, both in as-manufactured and machined conditions. The same scans taken through the top surface at 10 MHz include irregularities, such as grain scatter and returns from varying electron beam current distribution patterns programed into the build parameters. This leads to the premise that build direction and scan orientation affect the ability to identify defects in a sample at certain frequencies. It was shown, within the range of surface roughness available for this research, 10 MHz inspections are not affected by sample surface roughness to the extent that 2.25 and 5 MHz inspections. With the potential future use of AM for critical components, it is important to understand inspection techniques and the limitations associated with their use on AM materials.

References

Department of Defense (2014), *Nondestructive Inspection Methods, Basic Theory, T.O. 33B-1-1*, Robins Air Force Base: United States Air Force, GA.

Energetics Incorporated (2013), *Measurement Science Roadmap for Metal-Based Additive Manufacturing*, National Institute of Standards and Technology, Columbia.

Ford, S. (2014), "Additive manufacturing technology: Potential implications for US Manufacturing competitiveness", *Journal of International Commerce and Economics*, Vol. 6.

Hanks, E. (2016), "Surface roughness of electron beam melting TI-6AL-4V effect on ultrasonic testing", Thesis, Air Force Institute of Technology.

Hanks, E., Liu, D. and Palazotto, A. (2016), "Surface roughness of electron beam melting Ti-6Al-4v effect on ultrasonic testing", *57th AIAA/ASCE/AHS/ASC Structures, Structural Dynamics, and Materials Conference. 2016*.

İŞLEYİCİ, UMUT (2005), "Effect of surface roughness on ultrasonic testing", Thesis/Dissertation ETD, available at: www.citeseerx.ist.psu.edu/mwginternal/de5fs23hu73ds/progress?id=jazBIHuC6kMnLMl8LUcMWasvdX2hUX3Sa2SLaEUitIc,&dl (accessed 18 August 2017).

Levesque, D. (2016), *Review of Progress in Quantitative NDE*, by Chimenti, D.E. and Bond, L.J. (Eds), AIP Conf. Proc. 1706, New York, NY, Vol. 35, pp. 130003-1-9.

MathWorks (2015), *Matlab Documentation: Find Circles Using Hough Transform*, MathWorks, Natick.

Ruan, J. (2006), *A Review of Layer-Based Manufacturing Processes for Metals*, University of MO, Rolla.

Safdar, A. (2012), *A Study on Electron Beam Melted Ti-6Al-4V*, Lund University, Lund, Sweden.

Shipp, S. (2012), *Emerging Global Trends*, Institute for Defense Analyses, Alexandria.

Waller, J. (2014), *Nondestructive Evaluation of Additive Manufacturing: State-of-the-Discipline Report*, NASA Langley Research Center, Hampton.

Corresponding author

Anthony Palazotto can be contacted at: palazotto@sbcglobal.net